Scanning tunneling microscopy at the NbSe3 surface: Evidence for interaction between q(1) and q(2) charge density waves in the pinned regime

C. Brun, Zhao-Zhong Wang, Pierre Monceau

HAL Id: hal-00966555

https://hal.science/hal-00966555

Submitted on 26 Mar 2014

Scanning tunneling microscopy at the NbSe₃ surface: Evidence for interaction between $\mathbf{q_1}$ and $\mathbf{q_2}$ charge density waves in the pinned regime

Christophe Brun[*] and Zhao-Zhong Wang

Laboratoire de Photonique et de Nanostructures, CNRS, Route de Nozay, 91460 Marcoussis, France

Pierre Monceau

Institut Néel, Dept. MCBT, CNRS and University Joseph Fourier, 25 Avenue des Martyrs, BP 166, 38042 Grenoble Cedex 9, France

We have investigated both $\mathbf{q_1}$ and $\mathbf{q_2}$ charge density wave (CDW) states taking place in NbSe₃ by means of low-temperature scanning tunneling microscopy (STM) under ultrahigh vacuum on the *in situ* cleaved $(\boldsymbol{b},\boldsymbol{c})$ surface. High-resolution topographical images with atomic lattice resolution were obtained in the temperature range between 5 and 140 K. The careful and thorough analysis of the dependence of the STM images on bias polarity, energy, and temperature allowed us to identify unambiguously the three different types of chains composing the NbSe₃ unit cell at all temperatures, resolving contradictions from previous STM results. From two-dimensional Fourier transform of the STM images, we show that at the surface plane both CDW's wave vectors are in very good agreement with bulk reported values projected on the $(\boldsymbol{b},\boldsymbol{c})$ plane. The $\mathbf{q_1}$ CDW has, for wave vector, $\mathbf{q_1}=0.24\boldsymbol{b}^*$. Spatially, the $\mathbf{q_1}$ modulation is essentially developed on type III chains with a weak contribution on type II neighboring chains. The $\mathbf{q_2}$ CDW has, for wave vector, the projected value $\mathbf{q}_{2p}=0.26\boldsymbol{b}^*+0.5\boldsymbol{c}^*$. This modulation is mainly developed on type I chains but surprisingly has an important contribution on type III chains with an amplitude similar to the $\mathbf{q_1}$ contribution on these chains. This simultaneous double modulation on chain III leads to a beating phenomenon between the $\mathbf{q_1}$ and $\mathbf{q}_{2p}$ periodicities and gives rise to a new domain superstructure developed along the chain axis which is characterized by the vector $\boldsymbol{u}=2\times(\mathbf{q}_{2p}-\mathbf{q_1})-\boldsymbol{c}^*=2\times(0.26-0.24)\boldsymbol{b}^*$. We believe that these new features give a clue of the coupling between the $\mathbf{q_1}$ and $\mathbf{q_2}$ CDWs in the pinned regime. Whereas most studies investigated the various characteristics of both CDWs by probing the Nb atoms properties, our results are consistent with the interpretation according to which the electronic local density of states probed by STM is mostly that of the surface Se atoms.

I. INTRODUCTION

Many low-dimensional systems undergo a phase transition at a temperature called the Peierls temperature below which the electronic density is modulated and forms a charge density wave (CDW) with the wave vector $\mathbf{q}=2\boldsymbol{k}_F$ ($\boldsymbol{k}_F$ being the momentum at the Fermi level) concomitant with a periodic lattice distortion involving the same wave vector. Soon after its invention by Binnig *et al.* in 1982,[1] the scanning tunneling microscopy (STM) technique has been applied by Coleman *et al.*[2] for imaging directly the CDW in the real space at the surface of the quasi-two dimensional CDW compound 1T-TaS₂. Early experiments were performed in liquid media, encountering severe limitations to extract the intrinsic electronic properties at the surface. Recent STM measurements were reported in the last years on quasi-one dimensional CDW compounds, in improved experimental conditions under ultrahigh vacuum (UHV), allowing the discovery of new effects and new surface phenomena, including the results from our group on tetrathiafulvalene-tetracyanoquinodimethane (TTF-TCNQ) (Ref. 3) and on the blue bronze $K_{0.3}MoO_3$.[4–6] In the present work we have investigated by STM the CDW states, which occur in the one-dimensional compound NbSe₃. In contrast to the cases of TTF-TCNQ and $K_{0.3}MoO_3$, the opening of the CDW gaps in NbSe₃ only affects a part of the Fermi surface, the sample showing metallic resistivity down to very low temperature.

NbSe₃ was the first low-dimensional conductor discovered in which the CDW slides upon the application of a voltage above a threshold value leading to nonlinear transport properties.[7,8] It has become one of the most widely studied CDW systems.[9] NbSe₃ has a linear chain structure consisting of metallic chains running along the $\boldsymbol{b}$ axis, built of triangular prisms of selenium (Se) atoms having a niobium (Nb) atom at their center. Chains are staggered with respect to each other by half the height of the unit cell. Therefore besides the six selenium atoms of the MX_6 prism, each niobium is bonded to two more Se atoms from neighboring chains, and its coordination number is eight.[10,11] NbSe₃ crystallizes in a ribbonlike shape with the chain axis along $\boldsymbol{b}$, the ribbon being parallel to the $(\boldsymbol{b},\boldsymbol{c})$ plane. The typical size of the samples is a length of a several mm (even cm), a width along $\boldsymbol{c}$ of 10–50 μm, and a thickness of a few microns. There are six chains in the $P2_1/m$ monoclinic unit cell which are distinguished according to the strength of the chalcogen-chalcogen bond in the basis of the triangle of the chain. Chains with strong Se-Se pairing (Se₈-Se₉ distance of 2.37 Å) are called chains III; those with intermediate pairing (Se₂-Se₃ distance of 2.49 Å) are the chains I; and those with weaker bond (Se₅-Se₆ distance of 2.91 Å) are the chains II (see Fig. 1). However, the distance between the Se atoms from chains I and II (Se₃-Se₅) is only 2.73 Å, indicating a relatively strong coupling between these chains. NbSe₃ undergoes two successive Peierls transitions at $T_1=144$ K and $T_2=59$ K involving two different CDW wave vectors: $\mathbf{q_1}=0.24\boldsymbol{b}^*$ (high-temperature CDW) and $\mathbf{q_2}=0.5\boldsymbol{a}^*+0.26\boldsymbol{b}^*+0.5\boldsymbol{c}^*$ (low-temperature CDW). The lattice parameters at
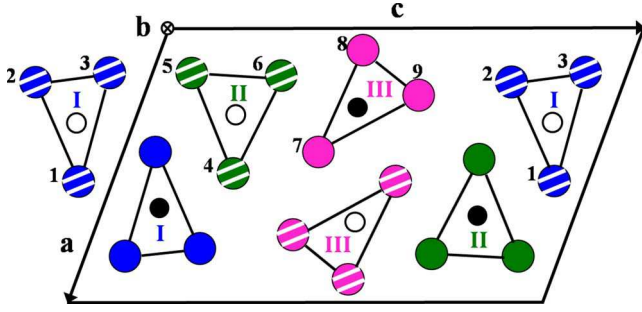
FIG. 1. (Color online) Projection of the unit cell of NbSe$_3$ perpendicular to the chain axis b. It consists of three pairs of chains labeled I, II, and III. Small and large circles denote Nb and Se atoms, respectively. Hatched Se atoms are lying at $z=0$ and full Se atoms at $z=b/2$. For each type of chain, the Nb atoms are displaced by $b/2$ from the Se atoms. At the (b,c) plane, the chains I, II, and III are lying, exposing the Se atoms at the surface after cleavage.

room temperature are $a=10.009$ Å, $b=3.48$ Å, $c=15.629$ Å, and $\beta=109.47°$.

Figure 1 shows the projection of the NbSe$_3$ unit cell (uc) perpendicular to the chain axis b. After cleavage, the top selenium atoms are the highest away from the (b,c) surface. The nearest niobium atoms from the surface are lying immediately below and are located at distances in the range 1.8–2.4 Å from the highest Se$_8$ atom. Due to this inequivalent crystalline surface structure inside the uc, the chains III are expected to be higher in STM images. However the distinction between the chains II and I will require a high spatial resolution to measure accurately the various Se-Se distances as well as the position of each chain with respect to chain III. Note that the Se atoms of chains I and II are displaced along by $b/2$ from the selenium atoms of chain III.

NMR (Refs. 12–14) and high-resolution x-ray diffraction[15] results show that q_1 CDW mainly affects the Nb atoms of chains III while q_2 CDW mainly affects the Nb atoms of chains I. Early STM experiments performed on the (b,c) plane of NbSe$_3$ were carried out in liquid media and three inequivalent types of chain could be identified.[16,17] Results obtained at 77 K did not give a clear evidence of the presence of the q_1 CDW in constant current STM images. Authors argued that, due to a poor signal to noise ratio, the q_1 modulation could only be detected on some STM scans along the b direction on one of the three chains which was therefore identified as chain III.[17] The 77 K results were inconsistent with the ones obtained at 4 K concerning the correct identification of chains I, II, and III. Results obtained at 4 K in liquid helium suggested that all three chains carry a strong CDW modulation.[17–19] A controversy arose because x-ray diffraction results showed that the largest displacive modulations occur on Nb(III) and Nb(I) while smaller displacive modulations affect the Se atoms of chains I, II, and III directly bonded to Nb(III) and Nb(I).[15] This discrepancy between x-ray diffraction and STM results, concerning the strong q_2 CDW modulation measured by STM on chains II, was partially solved by tight-binding calculations for a slab.[20] Due to the exponential decrease in the atomic-orbital amplitudes with distance, it was shown that STM should probe only the local density of states (LDOS) associated with

the surface Se atoms.[20] According to those calculations, chains II should also be involved in the q_2 CDW formation but STM should measure a smaller CDW amplitude on chains II than on chains I and III. Before our present work only one STM experiment was performed under UHV conditions, but at room temperature, i.e., in the normal state.[21]

In this study, we have investigated both q_1 and q_2 charge density wave states taking place in NbSe$_3$, in the temperature range between 5 and 140 K, by low-temperature scanning tunneling microscopy under ultrahigh vacuum on the *in situ* cleaved (b,c) surface. A preliminary report of the STM images at 5 K appeared.[22] The present results allow a clear identification of the three inequivalent chains existing inside a single unit cell at all temperatures. Using high-resolution STM images, the surface local distribution of the q_1 and q_2 CDWs on these elemental chains I, II, and III is carefully established. A consistent picture of the spatial distribution of both CDWs at all studied temperature on the three types of chains is obtained, together with a precise characterization of the CDW wave vectors at the surface. A surprising simultaneous double modulation is observed on chains III leading to a beating phenomenon between the q_1 and q_2 periodicities. This phenomenon gives rise to a new domain superstructure developed along the chain axis b which is characterized by the vector $u=2\times(0.26-0.24)b^*$. We suggest that these new features give a clue of the coupling between the q_1 and q_2 CDWs in the pinned regime.

II. EXPERIMENT AND RESULTS

A. Experimental setup

The present work was performed with an Omicron low-temperature UHV-STM system equipped with two UHV separated chambers. Well-characterized NbSe$_3$ single crystals with typical dimensions of $0.01\times10\times0.05$ mm^3 were selected. Samples were cleaved *in situ* at room temperature along the (b,c) planes; the optically flat (b,c) surface was carefully inspected before loading the sample into the STM head and finally slowly cooling down the system. Performing STM measurements on a cleaved NbSe$_3$ surface is tricky and delicate. First, because the sample width is only of tens of microns and second, because there always remain floating NbSe$_3$ fibers over the sample surface after cleavage, creating a risk for tip contamination. Both mechanically sharpened Pt/Ir tips and electrochemically etched W tips were used for the experiments leading to similar results. The q_1 and q_2 CDW states were studied from 5 to about 140 K both in cooling and in warming the system. All the STM images shown in the following are measured in constant current mode with the bias voltage applied on the sample.

B. STM on a quasi-one-dimensional metal

In the Tersoff-Hamann approximation, the tunneling current flowing between a metallic surface and the STM tip, and therefore the brightness of an STM image, is proportional to the local electronic density of states at the Fermi level (E_F), evaluated at the tip apex r_0, i.e., $\rho(r_0, E_F)$.[23] The situation of a quasi-one-dimensional metal is noticeably different from
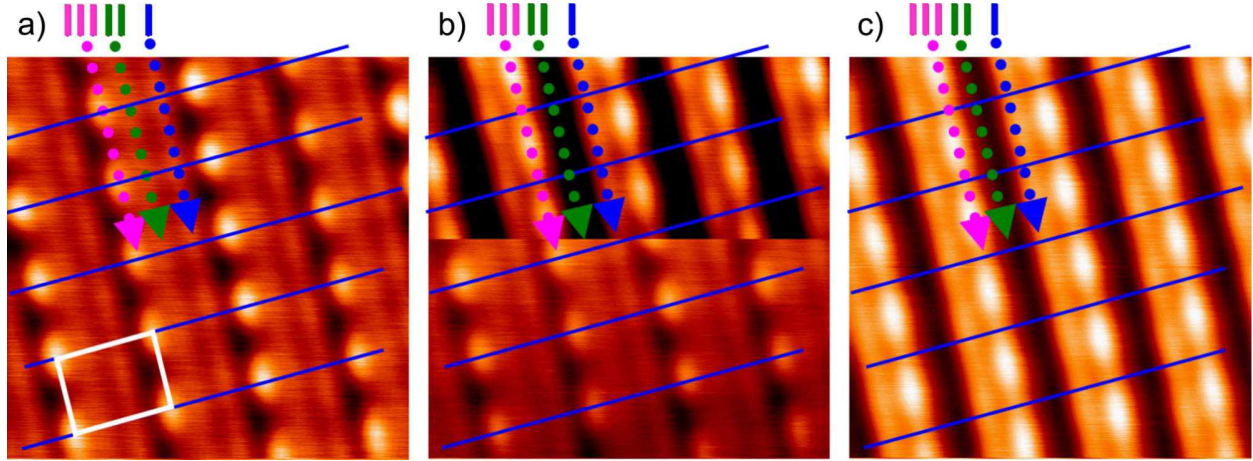
FIG. 2. (Color online) STM images of NbSe₃ (b,c) plane measured at 77 K on the same 7×7 nm² area, showing the dependency of the STM images on the polarity of the applied bias voltage. $I = 100$ pA. (a) $V_{bias} = +200$ mV. Three types of chains can be identified, one of them carrying a strong $\mathbf{q_1}$ CDW modulation and therefore identified as chain III. CDW modulation forms bright maxima along the chains, and the superlattice cell is indicated by a white rectangle. The two remaining chains are consistently identified as chains I and II. The transverse corrugation is of 0.2 Å and the $\mathbf{q_1}$ CDW corrugation is of 0.1 Å. (b) Change from $V_{bias} = +200$ mV in the bottom half of the image to $V_{bias} = -200$ mV in the upper half. There is a change of contrast on the chains II and only the chains I and III are clearly seen for $V_{bias} = -200$ mV. Maxima of CDW hole and electron states present a π phase shift (indicated by continuous lines), as expected for a quasi-one-dimensional system. (c) $V_{bias} = -200$ mV. Only chains I and III are clearly visible. Transverse corrugation is of 0.4 Å and $\mathbf{q_1}$ CDW corrugation is of 0.1 Å.

that of an isotropic metal. In particular the Fermi surface of quasi-one-dimensional materials is open and consists of warped cylinders with their axis perpendicular to the sheets, i.e., perpendicular to (b,c) planes for NbSe₃. In this situation, all electronic states available in the sample at E_F possess a finite $\mathbf{k_{\parallel}}$ wave vector. For small bias voltages, the tunneling transmission coefficient will be proportional, in a first approximation, to $\exp(-2z\sqrt{|\mathbf{k_{\parallel}}|^2 + \kappa^2})$,[23] where κ characterize the effective inverse length for the transmission coefficient to decrease along the direction perpendicular to the surface, z being the distance from the surface. It is seen that tunneling will favor the states with the lowest $|\mathbf{k_{\parallel}}|$ values. We evaluated the extremal values taken by $|\mathbf{k_{\parallel}}|$ for electronic states on the Fermi surface of NbSe₃, and we found that 0.23 Å$^{-1} \leq |\mathbf{k_{\parallel}}| \leq 0.30$ Å^{-1}, yielding a ratio of the extremal transmission coefficients equal to 1.3. This means that for NbSe₃ and for states close to E_F, the LDOS probed by STM is to a good approximation proportional to $\rho(\mathbf{r_0}, E_F)$ of the top layer.

The isocontours of $\rho(\mathbf{r_0}, E_F)$, that are measured in a constant current STM image, are governed by geometrical and electronic factors. The electronic factor is the LDOS of the surface atoms at the Fermi level. The geometrical factor is related to the exponential decrease in the atomic-orbital amplitudes with increasing distance from the surface. Thus, only the sample surface atoms closest to the tip that possess a non-negligible LDOS around E_F contribute the largest to the tunneling current and hence determine the contrast of the STM images. In the (b,c) plane of a single NbSe₃ layer, the surface Se atoms are expected to determine the $\rho(\mathbf{r_0}, E_F)$ isocontours because they are located several Å closer to the STM tip than the closest Nb atoms, although the LDOS on the Nb atoms is about five times larger than on the Se sites.[20]

C. STM results of the q₁ CDW phase

1. Polarity dependence of the images and identification of chains I, II, and III

At variance with STM results on TTF-TCNQ and K₀.₃MoO₃, as well as with former STM results on NbSe₃, we found that there is a dependency of the STM images on the polarity of the applied bias voltage, in usual tunneling conditions. Figure 2 shows three STM images of NbSe₃ taken at $T = 77$ K on the same 7×7 nm² area revealing this effect. At positive V_{bias}, when imaging the empty states of the sample (i.e., electrons tunneling out from the tip toward the sample), three different types of chains could always be identified. The $\mathbf{q_1}$ CDW modulation is clearly observed, the superlattice cell being indicated by a white rectangle [see Fig. 2(a)]. The observation that the $\mathbf{q_1}$ CDW is mainly developed on two different chains combined with the analysis of the mutual distances between neighboring chains allows us to identify the three different chains in terms of chains I, II, and III (color code adopted in the following to indicate the type of chain: pink for chains III, blue for chains I, and green for chains II). On the contrary, at negative V_{bias}, when imaging the occupied states (electrons tunneling out from the sample to the tip), the chains II were found to exhibit a lower LDOS and therefore only two types of chains are visible in the unit cell which are identified as chains I and III [see Fig. 2(c)]. The change of contrast on chains II from $V_{bias} = +200$ to $V_{bias} = -200$ mV is made explicit in Fig. 2(b). It should be noted that the maxima of the CDW corrugation are shifted by π between positive and negative bias voltages. This effect, of electronic origin, can be simply explained by analyzing the phase of the electronic wave functions of nearly free electrons submitted to a weak periodic one-dimensional
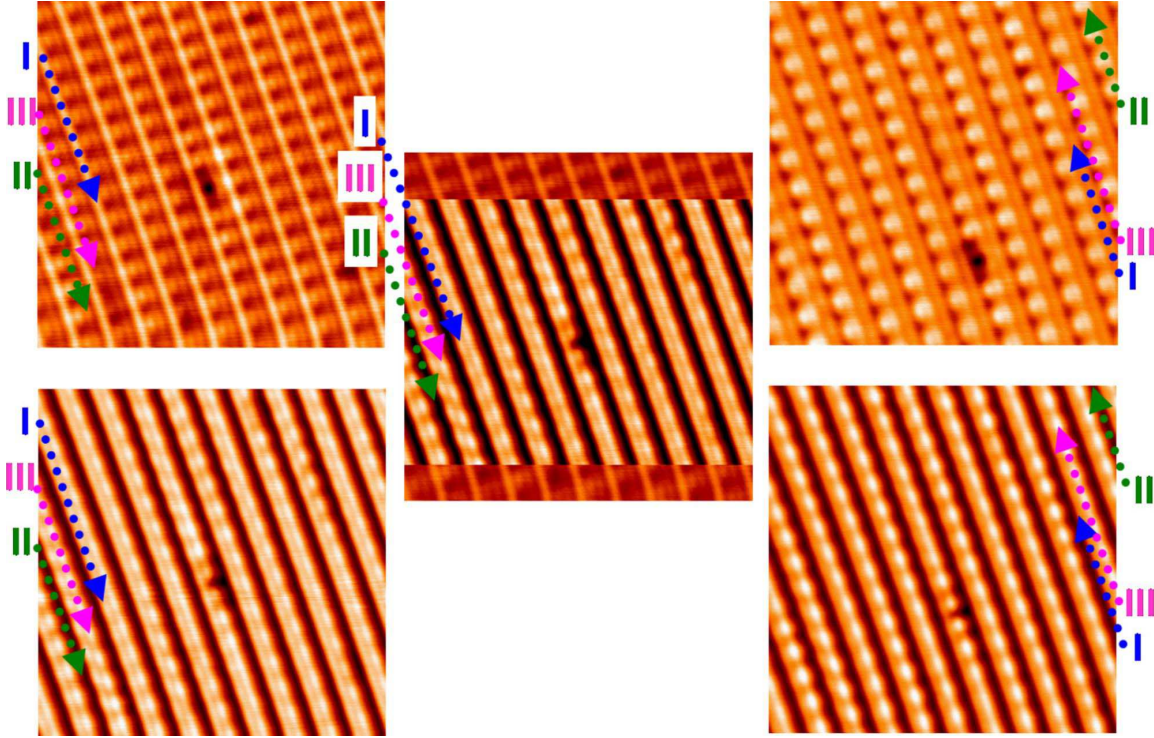
FIG. 3. (Color online) Dependence of the STM images on the probed energy of NbSe$_3$ ($\boldsymbol{b}$,$\boldsymbol{c}$) plane measured at 77 K on a 20 $\times$ 20 nm^2 area. Left images, top: V_{bias}=+100 mV; bottom: V_{bias}=−100 mV; right images, top: V_{bias}=+250 mV; bottom: V_{bias}= −250 mV. In the middle image, one can follow the change of polarity from +100 mV in the bottom, −100 mV in the median part, and +100 mV again in the top.

potential.[24] This effect has already been observed by STM in systems with additional periodic potential, and in particular in CDW systems.[25,26] The maxima of the CDW corrugation for $V_{bias}>0$ are indicated by parallel lines, becoming CDW minima for $V_{bias}<0$.

This dependence on the polarity occurs when the amplitude of V_{bias} is higher than 100 mV for a junction resistance typically on the order of 0.1–3 GΩ. For amplitudes lower than 100 mV, the contribution of the three chains can be detected for both polarities.

A possible explanation may be found in the particular band structure of NbSe$_3$. Several band structures have been proposed. It is considered that the band structure around the Fermi level consists of six bands originating from the dz_2 states of the Nb atoms, noticeably hybridized with the $4p$ states of highest energy of the Se atoms. Four of these bands cross E_F. All models attribute two of these six bands as originating mainly from the chains III. The two other bands with the highest energy—labeled b_1 and b_2 in Ref. 27—originate mainly from chains II. Different results have been presented concerning the position of these two bands with respect to E_F. Calculations of Bullet,[28,29] Shima,[30,31] and photoemission results of Schäffer et al.[32,33] found that the bottom of one of these two bands crosses E_F, leading to five bands crossing E_f. On the contrary, calculations of Canadell et al.[27] locate the fifth band above the Fermi level. In addition, the last two bands originating essentially from the Nb atoms of chains I are strongly hybridized with electronic states of chains II. One possibility to interpret the dependence on the polarity of the STM images would be, following the band-structure cal-

culations of Canadell et al.,[27] that one of the two empty bands, namely, b_1, would be nearly below the Fermi level with a minimum on the order of a few tens of mV. For any positive applied bias voltage, electrons could then tunnel out from the tip to the empty states of the chains II, making them visible in the STM images, as observed in the experiment. For negative V_{bias} the contribution of electrons tunneling out from chains II would be significant only for small bias voltages (on the order of the minimum of the b_1 band) and would decrease with increasing $|V_{bias}|$, with respect to the contribution of electrons tunneling out from chains I and III, as observed experimentally.

2. Energy dependence of the images

A change of contrast in the STM images occurs as a function of the amplitude $|V_{bias}|$ of the applied voltage whatever the polarity. At low energy, chains I are the highest in the STM image, while at higher energy, chains III are the highest. At 77 K the crossover occurs around 150–200 mV, i.e., in the energy range of the $\mathbf{q_1}$ CDW gap $2\Delta_1$.[32,34–37]

This effect is shown in Fig. 3 for both left images V_{bias} = $\pm$ 100 mV, and for both right images V_{bias}= $\pm$ 250 mV. In the central image, the polarity changes from +100 mV at the bottom to −100 mV in the middle part and to +100 mV again at the top. The three left images have been measured on the same zone, a defect being visible in the middle of the image. The two right images are slightly shifted, but with the same defect visible. In addition, the dependence on the polarity is clearly seen, as mentioned above. Both from the
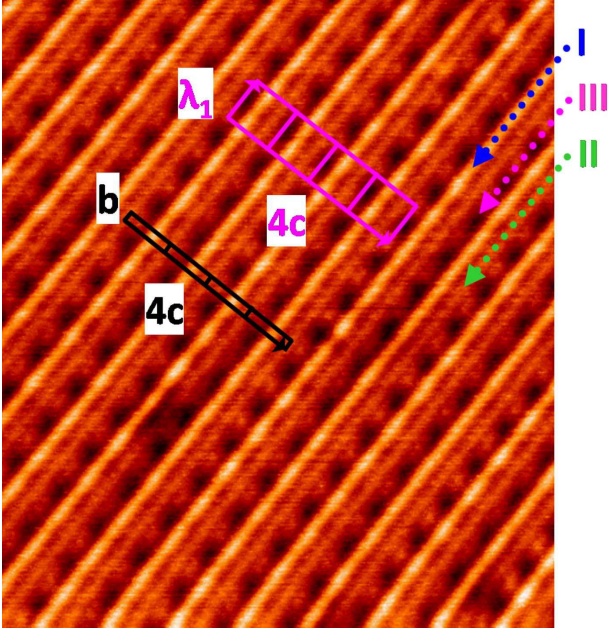
FIG. 4. (Color online) STM image of the $(\boldsymbol{b},\boldsymbol{c})$ plane of *in situ* cleaved NbSe$_3$ measured at 77 K. Scanned area: 20×20 nm^2. The atomic lattice corrugation is resolved and the corresponding unit cell is indicated together with the supercell of the $\mathbf{q_1}$ CDW. V_{bias} =+100 mV, I=1 nA.

FIG. 5. (Color online) 2D Fourier transform of the STM image is shown in Fig. 4. The lattice Bragg spots, corresponding to $\boldsymbol{b}^*$ and $\boldsymbol{c}^*$ reciprocal vectors are indicated by black arrows, and the $\mathbf{q_1}$ CDW superlattice spots are indicated by purple (light) vectors. STM measurements lead to $\mathbf{q_1}$=0.24$\boldsymbol{b}^*$ at the surface, in very good agreement with bulk reported values. Weaker superlattice spots associated to the $\mathbf{q_2}$ CDW are also visible at about 20 K above bulk transition temperature (see text).

surface crystallographic structure and the electronic structure, Ren and Whangbo[20] have shown that, in the Tersoff-Hamann approximation, chains III should dominate the LDOS around the Fermi level, due to the fact that their external Se$_8$ atoms are the nearest from the STM tip. For probed energies lower than $\simeq 2\Delta_1$, the LDOS on chains III is redistributed due to the opening of the CDW gap $2\Delta_1$ affecting essentially those chains; this explains why the chains I appear higher than chains III in this situation (see both left images of Fig. 3). The chains III become the highest in the STM images above an energy scale on the order of $2\Delta_1$ (see both right images of Fig. 3). A detailed theoretical analysis of the voltage dependency of the STM images was reported for the 2D compound 2H-NbSe$_2$.[38]

3. $\mathbf{q_1}$ CDW wave vector and resolution of the atomic lattice

Figure 4 shows a typical STM image of the empty states measured at 77 K with a bias voltage of +100 mV applied to the sample, i.e., close to the CDW gap edge value reported by other spectroscopic techniques.[32,34–37] The atomic lattice corrugation is resolved, although it appears not very clearly in the image for the $\boldsymbol{b}$ direction. However, the two-dimensional (2D) Fourier transform (FT) of this STM image presented in Fig. 5 clearly shows the lattice Bragg spots, attesting that the atomic lattice periodicity is resolved in the real-space image. The corresponding unit-cell vectors $\boldsymbol{b}$ and $\boldsymbol{c}$ are indicated, as well as $\lambda_1 = 2\pi/q_1$, the $\mathbf{q_1}$ CDW period. Three types of chain are clearly visible in the lattice uc and labeled according to our interpretation explained above. One of them carries strongly the $\mathbf{q_1}$ CDW modulation (chains III). We note that chains II are also modulated by the $\mathbf{q_1}$ CDW,
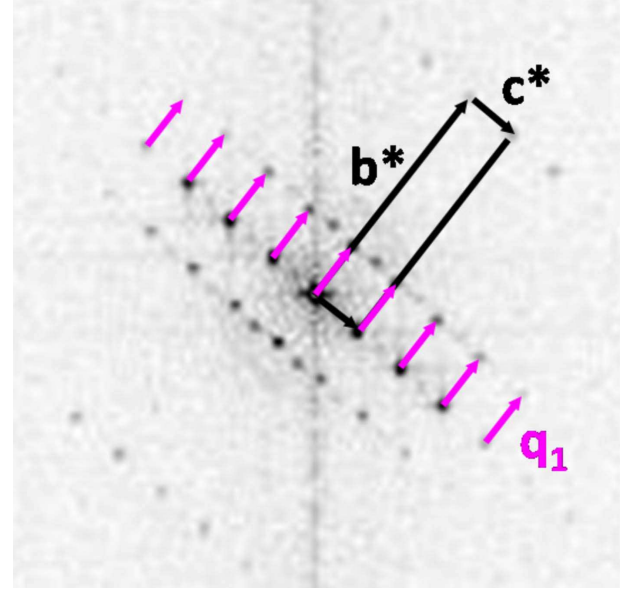
but with an amplitude around three to five times weaker than that on chains III. This is in agreement with x-ray diffraction results which show that Se atoms belonging to chains II and being the nearest Se atoms from chains III are modulated by $\mathbf{q_1}$ (Ref. 15) (Se$_6$ atoms in Fig. 1). The observed zero phasing between $\mathbf{q_1}$ periodicity on chains III and II suggests hybridization between the electronic states of the neighboring Se atoms of these two chains.

Figure 5 shows the 2D-FT of the image presented in Fig. 4. Both the surface lattice spots and the $\mathbf{q_1}$ CDW superlattice spots are observed. The simultaneous resolution of both the atomic lattice and the CDW allows to extract precisely the relation $\mathbf{q_1}$=0.24$\boldsymbol{b}^*$. This $\mathbf{q_1}$ value at the surface is in very good agreement with the 0.241$\boldsymbol{b}^*$ bulk value reported by x-ray diffraction experiments.[15] We note also the presence of satellites of smaller amplitude with vector $\mathbf{q_{2p}}$=0.26$\boldsymbol{b}^*$ +0.5$\boldsymbol{c}^*$, clearly visible around the central peak. They correspond to the $\mathbf{q_2}$ CDW projected on the $(\boldsymbol{b},\boldsymbol{c})$ plane. Observation of the $\mathbf{q_{2p}}$ superlattice spots at the surface of NbSe$_3$ almost 20 K above the Peierls temperature reported for the bulk, indicates that the $\mathbf{q_2}$ CDW ordering occurs at higher temperature at the surface than in the bulk.[39]

In some high-resolution images, one can detect locally a defect characterized by the occurrence of an extra CDW period on a particular chain, corresponding to a local dephasing of π of the CDW, i.e., a local loss of phase coherence. On the STM profile measured along this chain, it is observed that the CDW amplitude is strongly reduced at the position of this defect. This defect can thus be identified as an amplitude soliton. The interaction of the CDW with defects will be described in a following paper.[40]
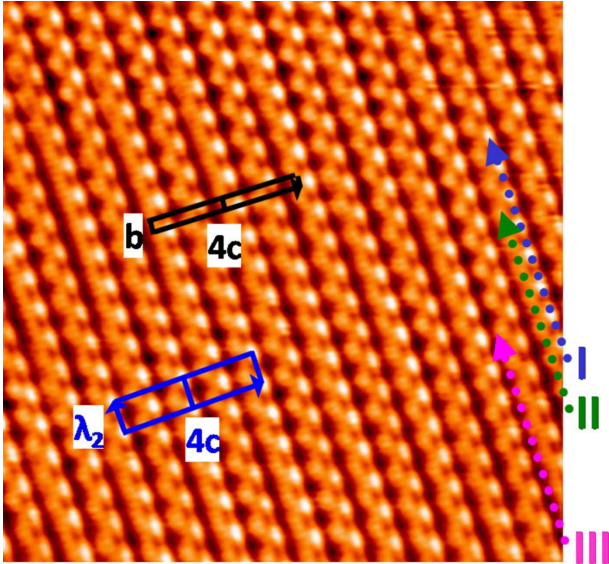
FIG. 6. (Color online) STM image of the ($\boldsymbol{b}$,$\boldsymbol{c}$) plane of *in situ* cleaved NbSe$_3$ measured at 5 K. V_{bias}=+200 mV, I=150 pA. Three types of chains are visible and the proposed identification of chains I, II, and III is consistent with our results obtained at 77 K shown in Figs. 2–4. The surface lattice unit cell and the $\mathbf{q_2}$ CDW surface supercell are indicated by black and blue (gray) arrows (λ_2 is the $\mathbf{q_2}$ period along the chain axis). Surprisingly the $\mathbf{q_2}$ CDW extends also on chains III making difficult the direct visualization of the $\mathbf{q_1}$ CDW superlattice in the image (see text). However the 2D Fourier transform of this image shown in Fig. 7 clearly shows its existence.

D. STM results of the coexisting $\mathbf{q_1}$ and $\mathbf{q_2}$ CDW phases

The STM results obtained at 5 K are consistent with those obtained at 77 K as far as the identification of the three types of chains, the dependence of the images on the polarity and on the energy are concerned. However, at 5 K the images are complex and the Fourier analysis reveals the presence of numerous spatial frequencies. Below T_2, $\mathbf{q_1}$ is found to yield the same value as at 77 K. Figure 6 shows an STM image measured at 5 K where both CDW superlattices as well as the underlying atomic lattice corrugation are resolved simultaneously. The $\mathbf{q_2}$ CDW is very visible on the image, the corresponding supercell being indicated. The $\mathbf{q_2}$ CDW superlattice affects essentially the chains I, but also to a less content, the chains II and III, as previously reported.[22] As at 77 K, three different chains are visible in the uc for $V_{bias}>0$. The chains on which the $\mathbf{q_2}$ modulation is essentially developed are identified as chains I. Analysis of the mutual distances between neighboring chains allows to distinguish chains II from chains III. As a surprising result, the $\mathbf{q_2}$ modulation is found to affect also the chains III. This has for consequence the observation of a "beating" phenomenon between the two slightly different periods of both CDWs along $\boldsymbol{b}^*$. This also allows to understand why the superlattice associated with $\mathbf{q_1}$ is no more directly visible in the STM images at 5 K, whereas it was easily seen at 77 K (see Figs. 2–4). Moreover when one carefully examines the STM images along the chains III, one can find a new long-range modulation which has an opposite phase on next-neighbor type III
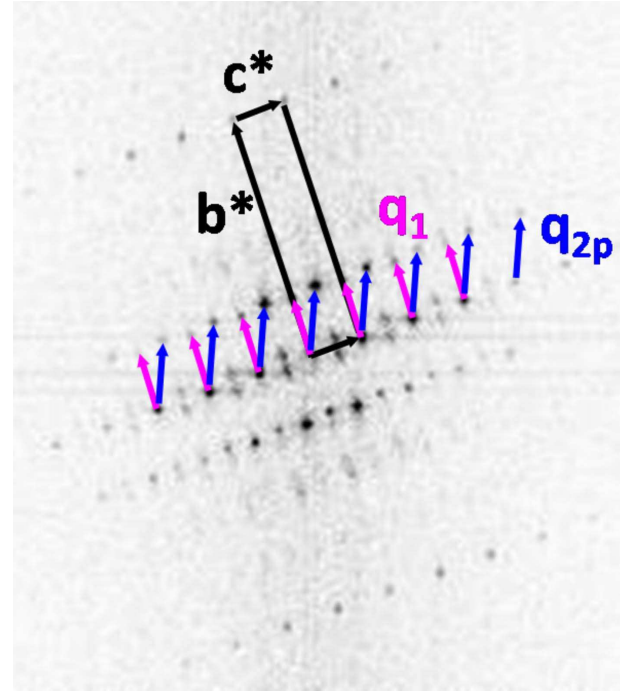

FIG. 7. (Color online) 2D Fourier transform of the STM image shown in Fig. 6. Lattice Bragg spots, corresponding to $\boldsymbol{b}^*$ and $\boldsymbol{c}^*$ reciprocal vectors are indicated by black arrows. $\mathbf{q_1}$ and $\mathbf{q_{2p}}$ CDW superlattice spots are indicated, respectively, by purple (light) and blue (gray) arrows. STM measurements yield $\mathbf{q_1}$=0.24$\boldsymbol{b}^*$ and $\mathbf{q_{2p}}$=0.26$\boldsymbol{b}^*$+0.5$\boldsymbol{c}^*$ in very good agreement with bulk reported values projected on the ($\boldsymbol{b}$,$\boldsymbol{c}$) plane.

chains (see Fig. 6). Profile analysis also shows that the $\mathbf{q_2}$ CDW modulates the chains II with an amplitude two or three times smaller than the one modulating chains I. $\mathbf{q_2}$ modulations are out of phase between the chains I and II that are immediate neighbors, as seen in Fig. 6.

The 2D-FT of the STM image of Fig. 6 is shown in Fig. 7. Bragg spots corresponding to the reciprocal vectors $\boldsymbol{b}^*$ and $\boldsymbol{c}^*$ (black arrows) associated with the atomic lattice are visible. Around them, $\mathbf{q_1}$ and $\mathbf{q_{2p}}$ satellite peaks are visible. The values found for the superlattice wave vectors are $\mathbf{q_1}$=0.24$\boldsymbol{b}^*$ and $\mathbf{q_{2p}}$=0.26$\boldsymbol{b}^*$+0.5$\boldsymbol{c}^*$. The accuracy of our measurements is such that one can distinguish the small difference between the $\boldsymbol{b}^*$ components of both CDWs: 0.24 and 0.26. The measured values of the wave vectors are independent of the probed energy, as expected for a CDW crystal. In addition to first harmonics, harmonics of order 2 and 3 for $\mathbf{q_1}$ and $\mathbf{q_{2p}}$ are seen, indicating that the two modulations are not purely sinusoidal. Second harmonics of $\mathbf{q_1}$ and $\mathbf{q_2}$ have been recently detected in high-resolution x-ray measurements using synchrotron radiation.[41]

To analyze in more details the spatial distribution of the various frequencies present in the STM images, we have filtered the FT of the images, keeping only the Fourier components to be studied by multiplying the original FT image by a suited filter. Using the linearity between FT and inverse Fourier transform (IFT),[42] Fourier filtering of the STM images allows to isolate the spatial contribution of the selected spectral components to the original image. The IFT images
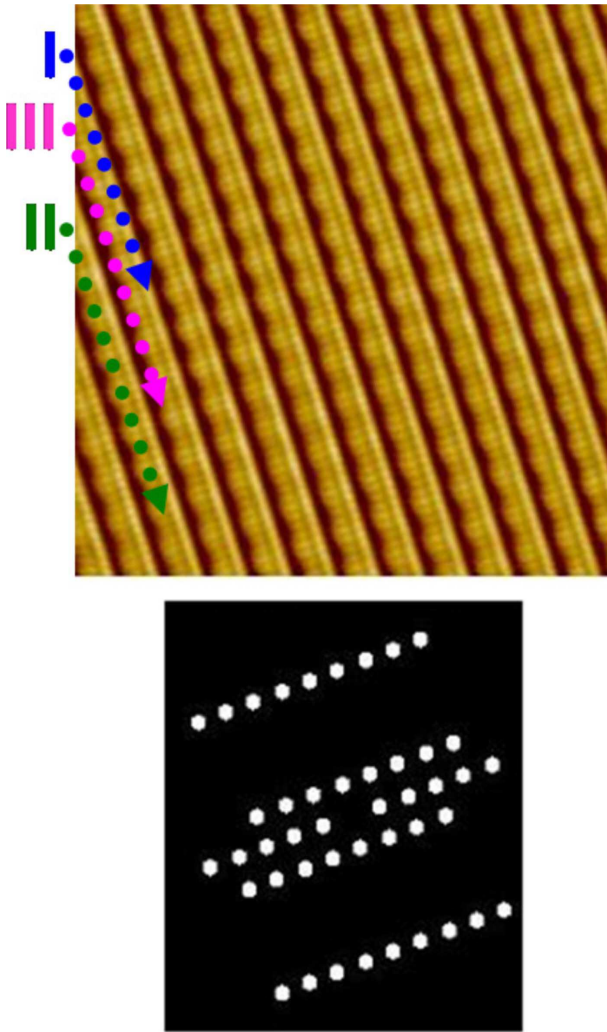
FIG. 8. (Color online) Inverse Fourier transform of Fourier-filtered STM image. This image is obtained from the original STM image shown in Fig. 6 by multiplying the band-pass filter indicated in black and white below the IFT image by the Fourier transform shown in Fig. 7 (white corresponds to values equal to one and black to zero). This procedure allows to disentangle the various spatial frequencies present in the original image. This filter keeps only the atomic lattice and the $\mathbf{q_1}$ CDW superlattice.
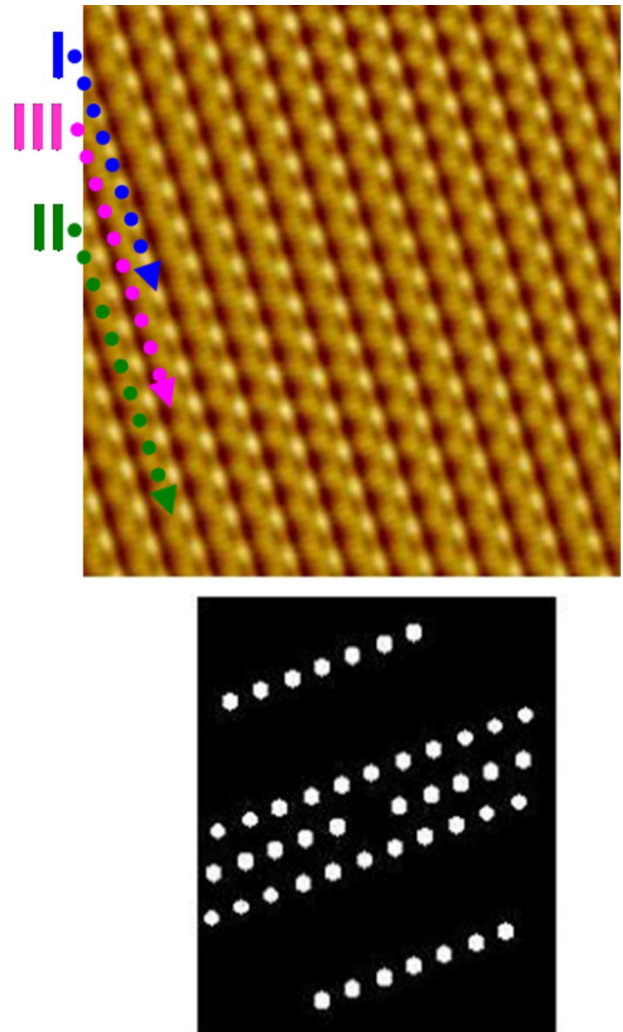

FIG. 9. (Color online) Same as in Fig. 8 but with a filter keeping only the atomic lattice and the $\mathbf{q_2}$ CDW superlattice.

obtained from the original image seen in Fig. 6 are shown in Figs. 8 and 9. The corresponding filters applied to the FT shown in Fig. 7 are presented below each IFT image. For each FT image, a filter consist of elementary circular band-pass filters, whose center is defined right at the maximum amplitude of the local Fourier spot to be band pass filtered. The radius of one elementary circular filter is defined in such a way that outside the circle, the amplitude of the remaining spectral components is within the background noise amplitude of the FT image. Inside the circle (outside the circle), the filter values are equal to one (zero) and a nonabrupt transition region from the ones to the zeros is defined to avoid numerical discontinuity. In Fig. 8, filtering keeps the atomic lattice (peaks written as $n\boldsymbol{b}^* + m\boldsymbol{c}^*$) and the superlattice associated with $\mathbf{q_1}$ (peaks written as $n\boldsymbol{b}^* + m\boldsymbol{c}^* + l\mathbf{q_1}$). The resulting IFT image shown in Fig. 8 displays very well the three

types of chains: I, II, and III. It is observed that the $\mathbf{q_1}$ CDW modulates essentially the chains III, with a modulation amplitude of 0.1 Å, in agreement with the results obtained at 77 K for comparable tunneling current and applied bias voltage (see Fig. 2). Chains II are also modulated by $\mathbf{q_1}$ with an amplitude three or four times smaller than that on chains III; this is also consistent with the results obtained at 77 K. This analysis also allows to see that the $\mathbf{q_1}$ CDW almost does not modulate the chains I.

In Fig. 9, filtering keeps the atomic lattice and the superlattice associated with the $\mathbf{q_2}$ CDW. It shows more clearly that, as described above, the $\mathbf{q_2}$ CDW modulates essentially chains I with an amplitude of 0.2 Å, and the neighboring chains II with an amplitude about three times smaller, both modulations being out of phase on immediate neighbor chains. More surprisingly, chains III are affected by the $\mathbf{q_2}$ CDW modulation. The corresponding amplitude is comparable to that of the $\mathbf{q_1}$ amplitude on these chains. This has for consequence the beating between both $\mathbf{q_1}$ and $\mathbf{q_2}$ periodicities (see next section).

Our results concerning the spatial distribution of $\mathbf{q_2}$ modulation on the three chains is qualitatively different from
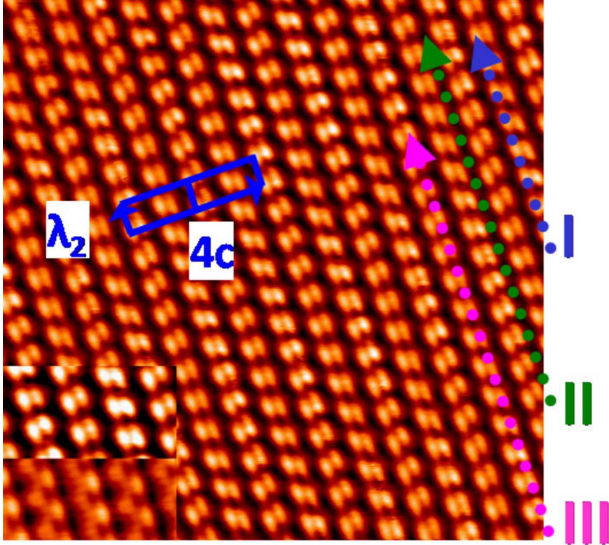
FIG. 10. (Color online) STM image measured at 5 K showing the same area as the one seen in Fig. 6 but showing here the occupied states. $V_{bias}=+200$ mV, $I=150$ pA. The inset in the bottom left part allows a detailed comparison with Fig. 6. It shows a smaller part of the same area, the bottom half being scanned with $V_{bias}=+200$ mV, the upper half with $V_{bias}=-200$ mV, highlighting the polarity dependence of chains II.

the results obtained by x-ray diffraction and NMR experiments. This is interpreted as a consequence of the fact that STM probes the energy integrated LDOS of the surface Se atoms and not that of the underlying Nb atoms, the latter being, however, more affected by the CDWs. It is possible that the surprising distribution of $\mathbf{q}_2$ on the three chains is due for one part to the strong hybridization between the electronic states of the Se atoms of chains I with those of the neighboring chains, and for a second part to the fact that these states are transversally more delocalized than those of chains III. For chains I this would yield electronic properties of the Bloch states based on Se atom orbitals qualitatively different from those based on the underneath Nb ones.

E. New long-range modulation of wave vector $u=2\times(\mathbf{q}_{2p}-\mathbf{q}_1)-\mathbf{c}^*$

As already mentioned above, an unexpected and surprising result indicates that on chains III the $\mathbf{q}_2$ modulation is present with an amplitude comparable to that of the $\mathbf{q}_1$ modulation. Figure 10 presents an STM image of the same area as scanned in Fig. 6, but showing the occupied NbSe$_3$ states ($V_{bias}=-200$ mV). The inset in the bottom left part of the figure allows easier comparison of Figs. 6 and 10. The polarity dependence, as reported before (see Figs. 2 and 3), is clearly seen. The FT of Fig. 10 is shown in Fig. 11. The comparison of the FT of the empty states image (see Fig. 7) with the occupied states image (see Fig. 11), shows the same lattice Bragg spots together with first-order CDW $\mathbf{q}_1$ and $\mathbf{q}_{2p}$ spots. However other new numerous satellite spots are seen in Fig. 11, including first, second, and third harmonics of $\mathbf{q}_1$ and $\mathbf{q}_{2p}$, as well as multiple combinations of $\mathbf{q}_1$ and $\mathbf{q}_{2p}$. Figure 12 shows a magnified view of the central part of the
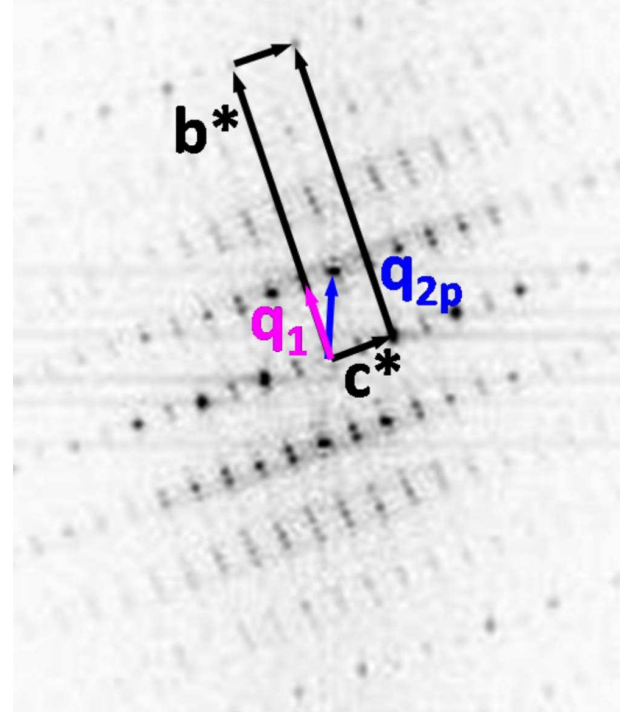

FIG. 11. (Color online) 2D Fourier transform of the STM image shown in Fig. 10. Lattice Bragg spots, corresponding to $\mathbf{b}^*$ and $\mathbf{c}^*$ reciprocal vectors, together with $\mathbf{q}_1$ and $\mathbf{q}_{2p}$ CDW superlattice spots are indicated. The same CDW wave vectors are found than in Fig. 7, in very good agreement with bulk reported values projected on the $(\mathbf{b},\mathbf{c})$ plane. New numerous satellite spots are observed including first, second, and third harmonics of $\mathbf{q}_1$ and $\mathbf{q}_{2p}$, as well as multiple combinations of $\mathbf{q}_1$ and $\mathbf{q}_{2p}$.

FT shown in Fig. 11. One can see harmonics of $\mathbf{c}^*$, $\mathbf{q}_1$, and $\mathbf{q}_{2p}$ with many other new satellite peaks. Among those, the most intense has an amplitude slightly lower than the $\mathbf{q}_1$ ones. They can be indexed as $m\mathbf{c}^*+2\times(\mathbf{q}_{2p}-0.5\mathbf{c}^*)-\mathbf{q}_1$ with m integer. The most intense peak of this type corresponds to $-2\times(\mathbf{q}_{2p}-0.5\mathbf{c}^*)+\mathbf{q}_1$ and is indicated in Fig. 12. One can observe that together with the $\mathbf{q}_1$ peaks, they form a "doublet" parallel to $\mathbf{b}^*$ separated by $\mathbf{u}=2(\mathbf{q}_{2p}-\mathbf{q}_1)-\mathbf{c}^*=2(0.26-0.24)\mathbf{b}^*$, indicated by short lines in Fig. 12. These new satellite peaks form bands parallel to $\mathbf{c}^*$. The first band is visible along the $m\mathbf{c}^*$ peaks (with m integer). These peaks can be indexed as $(m\mathbf{c}^*+\mathbf{q}_1-\mathbf{q}_{2p})$ and $(m\mathbf{c}^*-\mathbf{q}_1+\mathbf{q}_{2p})$. The doublet $\mathbf{u}$ separating these peaks is shown in the figure. The second and third bands are located where first-order and second-order $\mathbf{q}_1$ and $\mathbf{q}_{2p}$ satellites occur. The peaks can be indexed as: $(m\mathbf{c}^*+n\mathbf{q}_1+p\mathbf{q}_{2p})$ with m,n,p integers. None of these peaks, resulting from multiple combinations of $\mathbf{q}_1$ and $\mathbf{q}_{2p}$, were observed in x-ray or electronic diffraction experiments. Only the $\mathbf{q}_1$ and $\mathbf{q}_2$ second-order satellites were detected in high-resolution x-ray synchrotron radiation experiments.[41] The position of these peaks does not depend on the probed energy in the interval ±400 mV, although this new superstructure involves more harmonics for the occupied states images. This new superstructure appears at temperatures well below the occurrence of the $\mathbf{q}_2$ satellites and could be related to the self-energy renormalization of the band dispersion reported by photoemission below 50 K.[33]
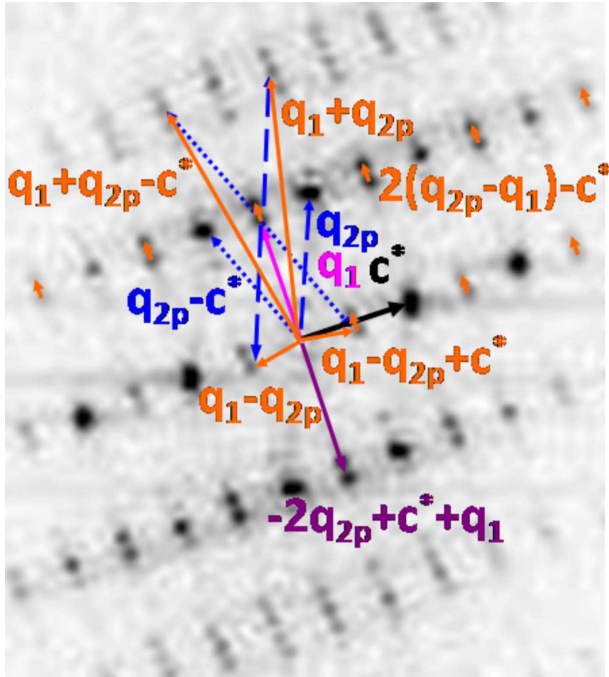
FIG. 12. (Color online) Zoom of the central part of the Fourier transform shown in Fig. 11. $\boldsymbol{c}^*$ reciprocal lattice vector together with the $\mathbf{q_1}$ and $\mathbf{q_{2p}}$ CDW wave vectors is indicated. Numerous superlattice peaks are visible, forming a superstructure involving both CDWs through the vector $\boldsymbol{u} = 2 \times (\mathbf{q_{2p}} - \mathbf{q_1}) - \boldsymbol{c}^*$, indicated by orange (light) short lines.

FIG. 13. (Color online) Inverse Fourier transform of Fourier-filtered STM images such as shown in Fig. 11 (sizes 20×20 nm² and 60×60 nm²). The band-pass filter being used is indicated on the upper right side (white corresponds to values equal to one and black to zero). This filter selects the atomic lattice and the doublet of satellite peaks formed by $\mathbf{q_1}$ and $2 \times (\mathbf{q_{2p}} - 0.5\boldsymbol{c}^*) - \mathbf{q_1}$. This procedure makes visible a domain superstructure developed on chains III, indicated by red arrows, which is hardly seen in original Fig. 10. The period is approximately defined by twice the difference in commensurability between the $\mathbf{q_1}$ and $\mathbf{q_2}$ CDW components along the chains, i.e., $\boldsymbol{u} = 2 \times (0.26 - 0.24)\boldsymbol{b}^* = 0.04\boldsymbol{b}^*$.

Using inverse Fourier transform of filtered STM images, it is shown that the new superlattice formed by the doublet of peaks $\mathbf{q_1}$ and $2 \times (\mathbf{q_{2p}} - 0.5\boldsymbol{c}^*) - \mathbf{q_1}$ is essentially developed on chains III. Figure 13 shows on 20×20 nm² and 60×60 nm² images that the resulting superstructure is a domain structure developed on chains III. These domains are indicated by arrows. Their characteristic period along $\boldsymbol{b}^*$ is equal to $7(\pm 1)\mathbf{q_1}$ periods, which corresponds approximately to $\boldsymbol{u} = 0.04\boldsymbol{b}^*$. These domains with a periodicity $\boldsymbol{u} = 0.04\boldsymbol{b}^*$ can be viewed as discommensurations along chains III, separating zones with the $\mathbf{q_1}$ periodicity. The analysis of this new superstructure benefited from the Fourier filtering procedure we have followed. Indeed, the comparison of the original Fig. 10 with the filtered Fig. 13 shows that this effect is difficult to be seen and analyzed in the original real-space STM image. This is because mainly one type of chain (chains III) is affected by this long-range modulation, while all three types of chains are at the same time spatially modulated by the CDWs.

The peaks corresponding to this new periodic superstructure defined by the vector $\boldsymbol{u}$ have not yet been reported in diffraction experiments. There is a possibility that this effect is specific to the energy integrated LDOS of the selenium atoms and does not exist for the deeper Nb atoms, which are more affected by the $\mathbf{q_1}$ and $\mathbf{q_2}$ CDWs. A reason for that might be the much lower hybridization between the Nb electronic states of different chains I, II, and III compared to that of the Se atoms. It is also possible that this effect occurs on
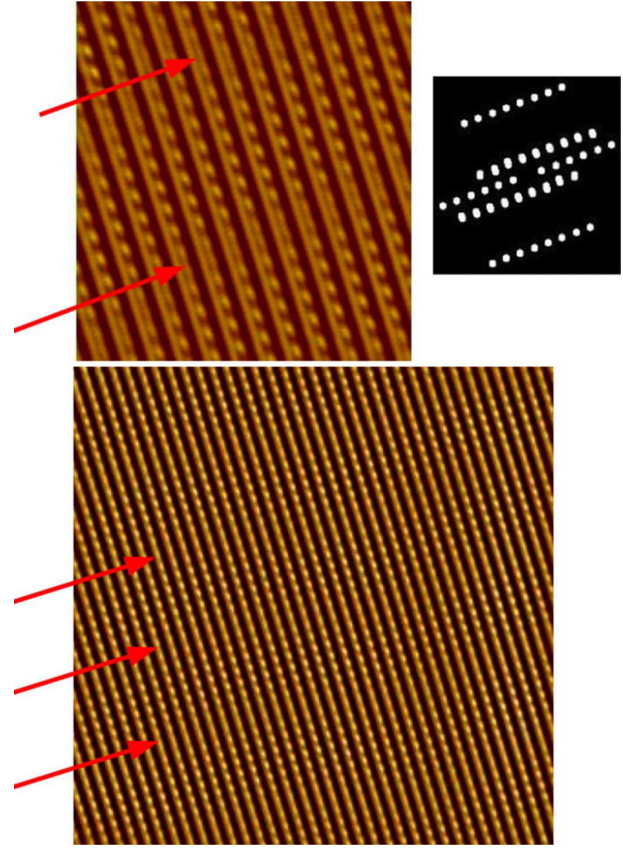
Nb atoms, but with a very small amplitude due to their weak mutual coupling, and is thus very difficult to detect experimentally. However, the structure factor of Nb and Se atoms is comparable, and the new modulation we have detected could bring a small detectable contribution in high-resolution x-ray diffraction experiment. NMR measurements on Se atoms could also reveal the existence of this coupling.

Is this coupling between $\mathbf{q_1}$ and $\mathbf{q_2}$ a surface effect or can it be detected in the bulk? Below T_2 a phase locking of the coexisting CDWs has been anticipated.[43] Indeed, the two NbSe₃ modulation wave vectors nearly satisfy the relation $2(\mathbf{q_1} + \mathbf{q_2}) \simeq (111) \equiv 0$ which suggests the possibility of a joint commensurability between the lattice and the two CDWs. However, no anomaly in the temperature dependence of $\mathbf{q_1}$ was detected[44] in the vicinity of T_2 and no lock-in transition to a true commensurate phase has been observed so far, implying that if a coupling exists, it is too small to be measurable, at least in the static (pinned) regime. Nevertheless, in the sliding state a dynamical electronic charge trans-

fer from the $\mathbf{q_1}$ to $\mathbf{q_2}$ condensate has been demonstrated, deduced from the Fermi-surface variation inferred from a concomitant shift of the $\mathbf{q_1}$ and $\mathbf{q_2}$ wave vectors.[45]

III. CONCLUSION

Using a UHV-LT-STM we have investigated the $(\boldsymbol{b},\boldsymbol{c})$ surface plane of the CDW compound NbSe$_3$, cleaved in UHV. We have studied both $\mathbf{q_1}$ and $\mathbf{q_2}$ CDW phases. The measured wave vectors at the surface are $\mathbf{q_1}=0.24\boldsymbol{b}^*$ and $\mathbf{q}_{2p}=0.26\boldsymbol{b}^*+0.5\boldsymbol{c}^*$, in excellent agreement with the bulk values reported by x-ray or electronic diffraction, projected on the $(\boldsymbol{b},\boldsymbol{c})$ plane. We have been able to identify the three types of chains present in the unit cell; we have clarified ambiguous previous STM results concerning this identification. Contrary to previous STM measurements, our results indicate clearly a dependence of the images on both polarity and probed energy. Thus when probing the empty states of NbSe$_3$, chains I, II, and III are visible while only chains I and III are observed when tunneling out of the occupied states. Following the available band-structure calculations, we have proposed the hypothesis that this polarity dependence of the LDOS probed in STM images, results from the specific position with respect to the Fermi level of the two bands associated with the electronic states of chains II. We have also proposed a redistribution of the spectral weight when the Peierls gaps are opened to explain the dependence of the images on the amplitude of the applied voltage: for voltage amplitude larger than the Δ_1 and Δ_2 gaps, chains III are seen predominantly in the STM images.

Below T_1 we have shown that the $\mathbf{q_1}$ modulation is essentially measured on chains III, with a small in-phase contribution on chains II, for $V_{bias}>0$, in agreement with x-ray diffraction results. Below T_2, STM images have a more complicated character because they include various spatial periodicities. Using the method of filtering the Fourier transform of STM images, we have shown that it was possible to characterize the spatial distribution of these various periodicities. For $T \leq T_2$, the $\mathbf{q_1}$ modulation remains essentially measured on chains III as for $T \geq T_2$; the $\mathbf{q_2}$ modulation is essentially measured on chains I, but with an important contribution on chains III with an amplitude similar to that of the $\mathbf{q_1}$ modulation. This result concerning the $\mathbf{q_2}$ distribution on the three types of chains is qualitatively different from the x-ray and NMR results probing the Nb atoms, the latter being more affected by the CDWs than the Se ones and also differently. Our results are consistent with the interpretation that in usual tunneling conditions the LDOS of the surface Se atoms is probed by STM, whereas that of the underlying Nb atoms contribute negligibly.

First-order, second-order, and third-order CDW satellite peaks have been observed in the Fourier transform of STM images, as well as new satellites peaks involving the wave vectors $m\boldsymbol{c}^*+n\mathbf{q_1}+p\mathbf{q_2}$, suggesting that some electronic states are modulated by both CDWs. Below T_2, the analysis of the Fourier transform of the STM images reveals that the superlattice associated with the $\mathbf{q_1}$ modulation becomes a superlattice of doublet peaks with $\mathbf{q_1}$ and $2\times(\mathbf{q}_{2p}-0.5\boldsymbol{c}^*)-\mathbf{q_1}$ wave vectors. A new superstructure of elementary wave vector $\boldsymbol{u}=2\times(\mathbf{q}_{2p}-\mathbf{q_1})-\boldsymbol{c}^*=0.04\boldsymbol{b}^*$ is observed, corresponding to twice the difference in commensurability between $\mathbf{q_1}$ and $\mathbf{q_2}$ along $\boldsymbol{b}^*$. Our analysis suggests that this effect essentially affects the chains III, which are modulated by both the $\mathbf{q_1}$ and $\mathbf{q_2}$ CDWs, giving rise to discommensuration domains of wave vector $\boldsymbol{u}=0.04\boldsymbol{b}^*$. These observations might be connected to the consequences in the real space of the self-energy renormalization of the band dispersion reported by photoemission below 50 K.[33]

The temperature dependence of the amplitude of the $\mathbf{q}_{2p}$ satellites shows that the $\mathbf{q_2}$ transition temperature occurs at the surface at a much larger temperature than in the bulk. This effect is described in a forthcoming paper.

*Present address: École Polytechnique Fédérale de Lausanne, Institut de Physique de la Matière Condensée, CH-1015 Lausanne, Switzerland.

[1] G. Binnig, H. Rohrer, C. Gerber, and E. Weibel, Appl. Phys. Lett. **40**, 178 (1982).

[2] R. V. Coleman, B. Drake, P. K. Hansma, and G. Slough, Phys. Rev. Lett. **55**, 394 (1985).

[3] Z. Z. Wang, J. C. Girard, C. Pasquier, D. Jérome, and K. Bechgaard, Phys. Rev. B **67**, 121401(R) (2003).

[4] C. Brun, J. C. Girard, Z. Z. Wang, J. Marcus, J. Dumas, and C. Schlenker, Phys. Rev. B **72**, 235119 (2005).

[5] E. Machado-Charry, P. Ordejón, E. Canadell, C. Brun, and Z. Z. Wang, Phys. Rev. B **74**, 155123 (2006).

[6] C. Brun, E. Machado-Charry, P. Ordejón, E. Canadell, and Z. Z. Wang, J. Phys.: Conf. Ser. **61**, 140 (2007).

[7] P. Monceau, N. P. Ong, A. M. Portis, A. Meerschaut, and J. Rouxel, Phys. Rev. Lett. **37**, 602 (1976).

[8] R. M. Fleming and C. C. Grimes, Phys. Rev. Lett. **42**, 1423 (1979).

[9] Proceedings of the International Workshops on Electronic Crystals (ECRYS): J. Phys. IV **9** (PR10) (1999); *ibid.* **12** (9) (2002); *ibid.* **131** (2005); Physica B **404** (3–4) (2009).

[10] A. Meerschaut and J. Rouxel, J. Less-Common Met. **39**, 197 (1975).

[11] J. L. Hodeau, C. Roucau, R. Ayroles, A. Meerschaut, J. Rouxel, and P. Monceau, J. Phys. C **11**, 4117 (1978).

[12] F. Devreux, J. Phys. (Paris) **43**, 1489 (1982).

[13] J. H. Ross, Jr., Z. Wang, and C. P. Slichter, Phys. Rev. Lett. **56**, 663 (1986).

[14] S. Suh, W. G. Clark, P. Monceau, R. E. Thorne, and S. E. Brown, Phys. Rev. Lett. **101**, 136407 (2008).

[15] S. van Smaalen, J. L. de Boer, A. Meetsma, H. Graafsma, H.-S. Sheu, A. Darovskikh, P. Coppens, and F. Levy, Phys. Rev. B **45**, 3103 (1992).

[16] G. Gammie, J. S. Hubacek, S. L. Skala, R. T. Brockenbrough, J. R. Tucker, and J. W. Lyding, Phys. Rev. B **40**, 9529 (1989).

[17] C. G. Slough, B. Giambattista, W. W. McNairy, and R. V. Coleman, J. Vac. Sci. Technol. A **8**, 490 (1990).

[18] C. G. Slough, B. Giambattista, A. Johnson, W. W. McNairy, and R. V. Coleman, Phys. Rev. B **39**, 5496 (1989).

[19] Z. Dai, C. G. Slough, and R. V. Coleman, Phys. Rev. Lett. **66**, 1318 (1991).

[20] J. Ren and M.-H. Whangbo, Phys. Rev. B **46**, 4917 (1992).

[21] A. Prodan, N. Ramšak, V. Marinković, S. W. Hla, F. W. Boswell, J. C. Bennett, and H. Böhm, Phys. Rev. B **54**, 10370 (1996).

[22] C. Brun, Z. Z. Wang, and P. Monceau, J. Phys. IV **131**, 225 (2005).

[23] J. Tersoff and D. R. Hamann, Phys. Rev. Lett. **50**, 1998 (1983).

[24] N. W. Ashcroft and N. D. Mermin, *Solid State Physics* (Saunders College, Philadelphia, 1976), Chap. 9, pp. 151–173.

[25] J. M. Carpinelli, H. H. Weitering, E. Plummer, and R. Stumpf, Nature (London) **381**, 398 (1996).

[26] P. Mallet, H. Guyot, J. Y. Veuillen, and N. Motta, Phys. Rev. B **63**, 165428 (2001).

[27] E. Canadell, E.-I. Rachdi, J.-P. Pouget, P. Gressier, A. Meerschaut, J. Rouxel, D. Dung, M. Evain, and M.-H. Whangbo, Inorg. Chem. **29**, 1401 (1990).

[28] D. W. Bullett, J. Phys. C **12**, 277 (1979).

[29] D. W. Bullett, J. Phys. C **15**, 3069 (1982).

[30] N. Shima, J. Phys. Soc. Jpn. **51**, 11 (1982).

[31] N. Shima, J. Phys. Soc. Jpn. **52**, 578 (1983).

[32] J. Schäfer, E. Rotenberg, S. D. Kevan, P. Blaha, R. Claessen, and R. E. Thorne, Phys. Rev. Lett. **87**, 196403 (2001).

[33] J. Schäfer, M. Sing, R. Claessen, E. Rotenberg, X. J. Zhou, R. E. Thorne, and S. D. Kevan, Phys. Rev. Lett. **91**, 066401 (2003).

[34] T. Ekino and J. Akimitsu, Jpn. J. Appl. Phys., Part 1 **26**, 625 (1987).

[35] Yu. I. Latyshev, P. Monceau, S. Brazovskii, A. P. Orlov, and T. Fournier, Phys. Rev. Lett. **95**, 266402 (2005).

[36] A. A. Sinchenko and P. Monceau, Phys. Rev. B **67**, 125117 (2003).

[37] K. O'Neill, E. Slot, R. E. Thorne, and H. S. J. van der Zant, Phys. Rev. Lett. **96**, 096402 (2006).

[38] W. Sacks, D. Roditchev, and J. Klein, Phys. Rev. B **57**, 13118 (1998).

[39] C. Brun, P. Monceau, and Z. Z. Wang (unpublished).

[40] C. Brun, S. Brazovskii, P. Monceau, and Z. Z. Wang (unpublished).

[41] P. Monceau, eSRF Report No. HS-2649 (unpublished).

[42] J. C. Russ, *The Image Processing Handbook*, 3rd ed. (CRC, Boca Raton, FL/Springer-Verlag GmbH, Heidelberg, 1999).

[43] R. Bruinsma and S. E. Trullinger, Phys. Rev. B **22**, 4543 (1980).

[44] A. H. Moudden, J. D. Axe, P. Monceau, and F. Levy, Phys. Rev. Lett. **65**, 223 (1990).

[45] A. Ayari, R. Danneau, H. Requardt, L. Ortega, J. E. Lorenzo, P. Monceau, R. Currat, S. Brazovskii, and G. Grübel, Phys. Rev. Lett. **93**, 106404 (2004).